Optimal Stochastic Scheduling Strategy of Multi-vector Energy Complex Integrated with Full-blown Power-to-biomethane Model

Guanwei Zeng, Chengxi Liu, Minfang Liao, Yongjian Luo, and Xuzhu Dong

Abstract—**We propose an optimal stochastic scheduling strategy for a multi-vector energy complex (MEC), considering a full-blown model of the power-to-biomethane (PtM) process. Unlike conventional optimization that uses a simple efficiency coefficient to coarsely model energy conversion between electricity and biomethane, a detailed PtM model is introduced to emphasize the reactor kinetics and chemical equilibria of methanation. This model crystallizes the interactions between the PtM process and MEC flexibility, allowing to adjust the operating condition of the methanation reactor for optimal MEC operation in stochastic scenarios. Temperature optimization and flowsheet design of the PtM process increase the average selectivity of methane (i.e., ratio between net biomethane production and hydrogen consumption) up to 83.7% in the proposed synthesis flowsheet. Simulation results can provide information and predictions to operators about the optimal operating conditions of a PtM unit while improving the MEC flexibility.**

Index Terms—**Multi-vector energy complex, optimal stochastic scheduling, power-to-biomethane unit, process synthesis, natural gas.**

I. Introduction

RECENTLY, the global crisis of natural gas supply has intensified owing to the interweaving of global geopolitical risks and various adverse circumstances [1]. The natural gas consumption in 2021 was 4.0 trillion cubic meters worldwide, with a yearly growth rate of approximately 5.3%. The remaining recoverable natural gas reserves in the world are estimated to be only 192 trillion cubic meters [2]. To alleviate this crisis, the power-to-biomethane (PtM) process, an electrical-chemical energy conversion technology, is attracting growing interest because high-quality biomethane is a promising alternative to natural gas. PtM units play a substantial role in cross-sector integration, possibly leading to sustainable multi-vector energy complexes (MECs). However, the integration of the individual PtM procedures (i.e., water electrolysis and methanation) into an MEC remains an important open problem.

Over the past few years, the optimal operation of MECs has been investigated considering the power-to-gas process represented by a conversion coefficient. Existing studies generally differ in terms of the objective function, uncertainty management, and energy conversion units. Typically, an optimal dispatch model employs operation cost minimization as the objective function [3]-[5]. In addition, multi-objective optimization has been explored to simultaneously minimize operation costs and emissions in response to environmental and social concerns [6]-[8]. In [3], a PtM unit, hydrogen fuel cell, and combined heat and power (CHP) system were modeled to flexibly transform among electricity, hydrogen, and natural gas, thereby guaranteeing energy supply in residential energy systems. Other energy conversion facilities such as biomass pools, biogas boilers, and pyrolysis gasification can be modeled to integrate bioenergy systems into traditional multi-energy structures [9], [10]. In addition, the interest in applying stochastic analysis to multiple energy systems is growing. Considering several uncertainties, [8] proposed a convex-set-based stochastic algorithm to handle the volatility of renewables and optimize day-ahead operations of a PtM-based multi-energy system. Reference [11] proposed a risk-constrained stochastic scheduling strategy to leverage the latent scheduling capacity of a multi-energy system toward economic operation while maintaining the system operation risk level under uncertain renewable generation. Reference [12] proposed a two-stage stochastic formulation with mixed-integer conic programming recourse decisions involving holistic investment and operation modeling. It aimed to optimally locate and configure microgrids with hydrogen fueling stations. The fluctuating electricity prices and demand were also considered by employing an improved spectral clustering method in [13]. Despite the various scheduling strategies proposed to address the coordination among energy supply, conversion, and consumption, and even considering uncertainties, a PtM unit has not been properly modeled or incorporated to capture the interactions between its operation and the MEC flexibility in stochastic scenarios.

Although natural gas alleviates the storage and delivery of hydrogen, extensive research has been conducted on metha-

Manuscript received: November 8, 2022; revised: April 26, 2023; accepted: June 24, 2023. Date of CrossCheck: June 24, 2023. Date of online publication: July 28, 2023.

This work was supported by the National Key R&D Program of China "Large-scale energy storage systems based on high temperature solid oxide electrolysis cells and biogas methanation technologies" (No. 2021YFE0191200).

G. Zeng, L. Liu (corresponding author), M. Liao, Y. Luo, and X. Dong are with Hubei Engineering and Technology Research Center for AC/DC Intelligent Distribution Network, Wuhan, China, and they are also with the School of Electrical Engineering and Automation, Wuhan University, Wuhan, China (e-mail: zengguanwei@whu.edu.cn; liuchengxi@whu.edu.cn; liaominfang@whu.edu.cn; yongjianluo@whu.edu.cn; dongxz@whu.edu.cn).

DOI: 10.35833/MPCE.2022.000741

nation for hydrogen-to-methane generation as a result of hydrogen production. In particular, biogas methanation, in which carbon dioxide (CO_2) feedstock is provided by biogas, has received increasing attention. Reference [14] developed a dynamic methanation unit model to match variable hydrogen production powered by intermittent renewable electricity. Based on the methanation unit model, the number of required methanation reactors and volume of CO_2 infeed were optimized to broaden the rangeability of the PtM unit [15]. In [16], a model integrating a PtM unit and biogas plant was constructed, allowing the analysis of feedstock gate fees and uncertain renewable energy source (RES) generation for system operation. Reference [17] developed a superstructure optimization model for methane synthesis to establish an electrothermal hybrid process with a high overall system efficiency. Experiments based on a full-scale model of a methanation reactor showed that a sub-stoichiometric ratio of 3.9 was the optimal value to obtain high-quality biomethane as a substitute for natural gas [18].

Existing studies have focused on the independent operation and optimization of methanation. MECs can be regarded as energy hubs between distributed energy grids and consumers. PtM units are essential in MECs because they influence multiple systems (e.g., electricity, natural gas, and heating systems) [19], [20]. Hence, methanation should be integrated into MECs for scheduling from a systematic perspective. Nevertheless, the corresponding chemical processes can lead to high complexity of the model if they are directly inserted into the optimal scheduling problem of MECs. Hence, a concise PtM model should be devised from the complicated chemical processes for better integration into optimal scheduling of an MEC. To this end, we developed a detailed model of methane synthesis and integrated it into an MEC. Then, an optimal day-ahead scheduling model was derived considering ① the mutual coordination between diverse energy vectors at both the supply and demand sides through several energy conversion units, ② a detailed representation of chemical PtM processes, and ③ uncertainties introduced by RES generation and energy demand.

The main contributions of this paper are summarized as follows.

1) An MEC is established covering energy purchase, storage, distribution, and supply, as well as energy conversion between electricity, natural gas, hydrogen, biomethane, heating, and cooling, thus enabling diverse, flexible, and secure energy flows.

2) A detailed model of methane synthesis is designed and integrated into the MEC considering its chemical process. This model establishes a new paradigm for the joint regulation of the PtM unit and MEC. Various operating conditions are optimized, including the temperature of the methanation reactor, biomethane conversion rate, and total cost (TC) of the MEC.

3) A scenario-based stochastic scheduling strategy is formulated to convert the uncertainties introduced by RES generation and energy demand into multiple determined scenarios for separate optimization. Thus, the expected cost in all scenarios is reduced.

The remainder of this paper is organized as follows. Section II describes the MEC and PtM modeling. The overall problem formulation and solution are detailed in Section III. Case studies are presented in Section IV, and conclusions are drawn in Section V.

II. MEC and PtM Modeling

A. MEC Structure

We propose an MEC structure containing a full PtM model, as shown in Fig. 1. The electricity input of the MEC is supplied by the distribution networks, RESs (e.g., wind and solar) [21], and energy storage (ES) system [22], whereas natural gas is provided by the underlying networks. Through different energy conversion units, i.e., CHP units, electrolyzers, methanators, electrical heat pumps (EHPs), gas furnaces, and chiller boilers, the supplied electricity and natural gas are transformed and coordinated to fulfill four types of demands: electricity, natural gas, heating, and cooling. The variables in Fig. 1 are defined in Appendix A Table AI and AII.

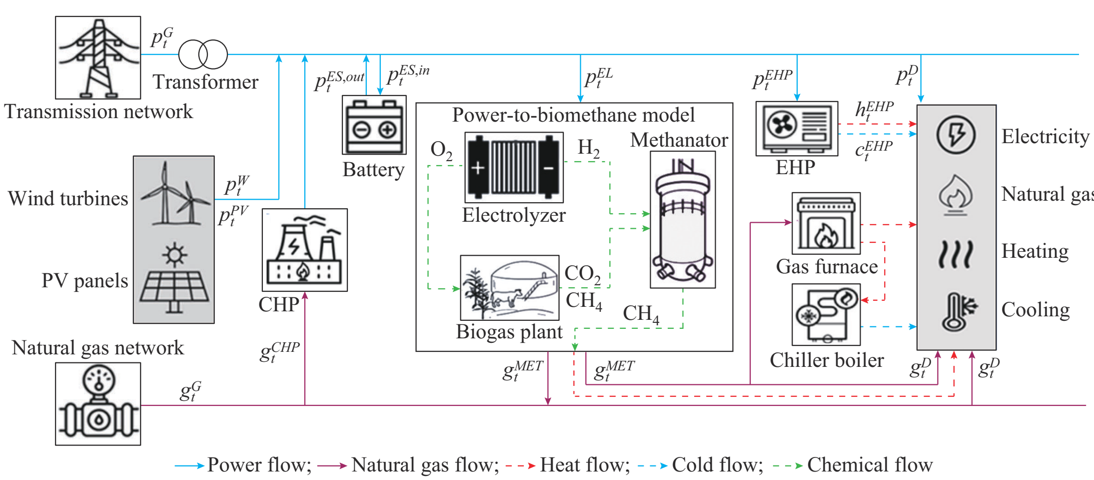

Fig. 1. Proposed MEC structure containing a full PtM model.

As an energy conversion component in an MEC, the PtM unit has been a research hotspot owing to its functions of ① energy sector integration, ② CO_2 and waste reduction, and ③ RES accommodation [23]. The product gas (synthetic gas), biomethane, is obtained either from methanation or by upgrading the biogas produced from the anaerobic digestion of wet biomass, mainly consisting of 50-70% methane and 30-50% CO_2 [24]. The difference among biomethane extraction methods is that the methanation path exploits the CO_2 contents to a large extent by hydrogenation rather than elimination, thus reducing CO_2 emissions. As biomethane can fuel natural gas facilities [25], it increases the MEC flexibility. For example, curtailed RES infeed can be transformed into biomethane for downregulation, whereas during peak demand hours, biomethane can fuel CHP units to back up the electricity supply.

The PtM process shown in Fig. 2 consists of four steps: ① electrochemical water splitting, ② biogas production, ③ cleaning, and ④ CO_2 methanation. In this paper, we focus on the mathematical modeling of electrochemical water splitting and CO_2 methanation.

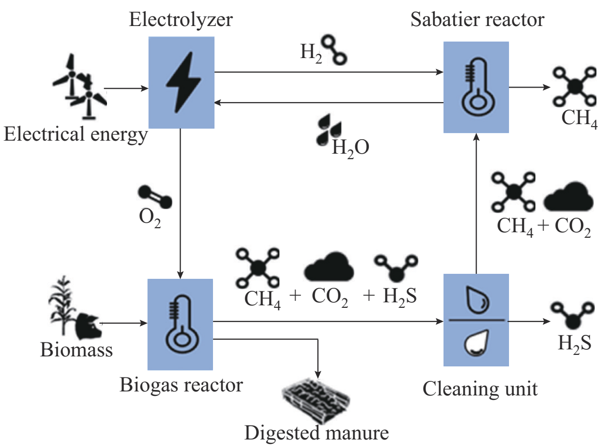

Fig. 2. Schematic of PtM process.

B. Mathematical Model of Water Electrolysis

Water electrolysis involves water, electrical energy, and heat energy as the inputs and hydrogen as the main product. The chemical equation is given by:

$$H_2O + \text{heat} + \text{electricity} \rightarrow H_2 + O_2 \tag{1}$$

The theoretical energy required for this process (i. e., enthalpy ΔH of the reaction) is derived from thermodynamics, which describes the ideal case of the water electrolysis as:

$$\Delta H = \Delta G + T\Delta S \tag{2}$$

where ΔG is the Gibbs free energy, indicating the minimum amount of electrical energy needed; and $T\Delta S$ is the entropic heat consumption dependent on the cell temperature T.

The energy required for the reaction is higher than the theoretical one (i.e., ΔG) owing to various losses such as activation loss η_{act}, ohmic loss η_{ohm}, and concentration loss η_{conc}, which can be expressed in the voltage of the electrolyzer cell as:

$$U_{cell} = U_{rev} + \eta_{act} + \eta_{ohm} + \eta_{conc} \tag{3}$$

where U_{rev} is the reversible voltage of the electrolyzer cell.

This voltage inefficiency generates irreversible Joule heat in the electrolyzer, which is expressed as the product of current I and the loss-induced voltages:

$$\dot{Q}_{ir} = I\left(\eta_{act} + \eta_{ohm} + \eta_{conc}\right) \tag{4}$$

Part of the heat is dissipated to the environment, denoted as:

$$\dot{Q}_{loss} = \left(T - T_0\right)\alpha_{AC} S_{AC} \tag{5}$$

where α_{AC} and S_{AC} are the construction-specific parameters of the electrolyzer cell; and T_0 is the environment temperature.

Hence, the heat required by the electrolyzer $\dot{Q}_{cell}$ can be calculated as:

$$\dot{Q}_{cell} = T\Delta S - \left(\dot{Q}_{ir} - \dot{Q}_{loss}\right) \tag{6}$$

When the heat generation within the electrolyzer is larger than entropic heat $T\Delta S$, net heat is produced because the entropic heat consumption is fully offset by the irreversible heat production. Nevertheless, heat should be supplied by an external source because there is net heat consumption.

Therefore, the efficiency of water electrolyzer η_{EL} is defined by the ratio of output chemical energy to the total input energy as:

$$\eta_{EL} = \frac{\dot{N}_{H_2,out} C_{HHV}}{E/\eta_{con} + \dot{Q}_{cell} + \dot{Q}_{H_2O}} \tag{7}$$

where $\dot{N}_{H_2,out}$ is the hydrogen production rate [26]; C_{HHV} is the higher heating value of hydrogen, which remains constant; E is the electrical energy consumed by the electrolyzer; and η_{con} is the converter efficiency. The energy used to heat freshly added water to the stack temperature is given by:

$$\dot{Q}_{H_2O} = \dot{m}_{H_2O}\left(T - T_{H_2O}\right)c_{H_2O} \tag{8}$$

where $\dot{m}_{H_2O}$ is the mass of the freshly added water per unit time; and c_{H_2O} is the heat capacity of water. Hence, the chemical power of the output hydrogen and power input linked by the efficiency can be expressed as:

$$f_{H_2,t} = p_t^{EL}\eta_{EL}\xi \tag{9}$$

where ξ is the unit conversion factor from megawatts to kilograms per second. The power input of the electrolyzer p_t^{EL} is bounded by its load range:

$$\underline{p}_{EL} \leq p_t^{EL} \leq \bar{p}_{EL} \tag{10}$$

where $\underline{p}_{EL}$ and $\bar{p}_{EL}$ are the lower and upper limits of the load range of electrolyzer, respectively.

C. Mathematical Model of Methanation

With hydrogen produced from water electrolysis and CO_2-contained biogas provided by a biogas plant, biomethane can be generated in a methanator. Figure 3 shows the flowsheet of methane synthesis, through which the stream along the input and output of each unit should follow the mass balance given by:

$$F_z = \sum_{c \in C} f_{c,z} \quad \forall z \in Z, \forall c \in C \tag{11}$$

$$f_{c,z} = F_z \delta_{c,z} \quad \forall z \in Z, \forall c \in C \tag{12}$$

where F_z is the total mass flow of stream z; $f_{c,z}$ is the mass flow rate of component c in stream z (e.g., hydrogen, oxygen, or methane flow); $\delta_{c,z}$ is the mass fraction of component c; Z is the set of all streams; and C is the set of all the components in the methanator. The heating value of stream z is the sum across components c, which is calculated as the product of mass flow rate $f_{c,z}$ and its standard enthalpy of formation (the two terms in parentheses):

$$\dot{Q}_z=\sum_c f_{c,z}\left(\Delta H_{f,c}^0+\int_{T_0}^{T} Cp_c(T)\,\mathrm{d}T\right)\quad \forall z\in Z,\forall c\in C \tag{13}$$

where $\Delta H_{f,c}^0$ is the standard enthalpy of formation; and Cp_c is the heat capacity of gas component c, which depends on the temperature of electrolyzer and heat capacity constants [27]. Equations (11) - (13) define the global methanation constraints. The characteristic equations of the individual facilities in the flowsheet are described below.

First, the electrolytically generated hydrogen with an approximate temperature of 600 °C is cooled down through a heat exchanger. The cooling process should satisfy the following mass balance equation, indicating that the mass fraction of each component remains the same:

$$\delta_{c,z}=\delta_{c,z'}\quad \forall z\in HXO,\forall z'\in HXI \tag{14}$$

where HXO and HXI denote the output and input flows of the heat exchanger, respectively.

The heat removed by the heat exchanger can be expressed as:

$$\dot{Q}_{hx}=\dot{Q}_{z'}-\dot{Q}_z\quad \forall z\in HXO,\forall z'\in HXI,\forall hx\in HX \tag{15}$$

where HX is the set of all the heat exchangers. Two similar heat exchange units (HX2 and HX3 in Fig. 3) are employed later in this process. HX2 adjusts the temperature for better methane synthesis, and HX3 cools down the product gas from the reactor to facilitate condensation.

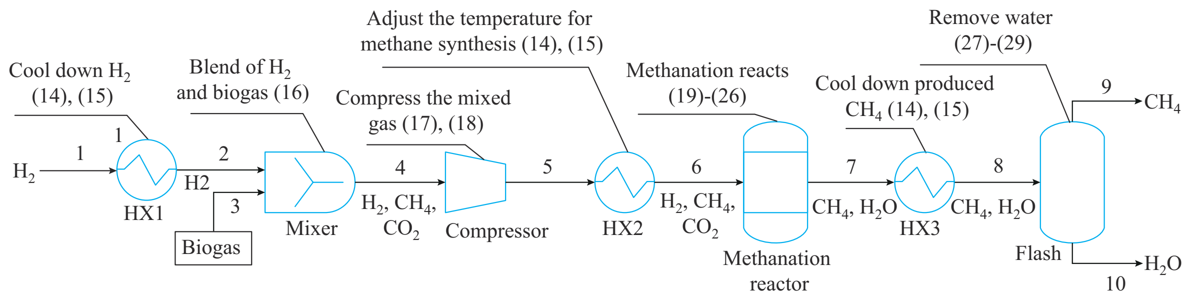

Fig. 3. Flowsheet of methane synthesis.

Hydrogen and biogas are then blended in a mixer unit, and the temperature of the mixed outlet stream is calculated based on the energy balance equation as:

$$\dot{Q}_z=\sum_{z'}\dot{Q}_{z'}\quad \forall z\in MO,\forall z'\in MI \tag{16}$$

where MO and MI are the output and input of the mixer, respectively.

Subsequently, the mixed gas is delivered to the compressor to reach the desired pressure. The power consumption and discharging temperature can be calculated as:

$$W_{comp}=F_{z'}\frac{8.314T_{z'}}{M_{gas}\eta}\frac{k}{k-1}\left[\left(\frac{p_z}{p_{z'}}\right)^{\frac{k-1}{k}}-1\right]\quad \forall z\in CO,\forall z'\in CI \tag{17}$$

$$T_z=T_{z'}+T_{z'}\left[\left(\frac{p_z}{p_{z'}}\right)^{\frac{k-1}{k}}-1\right]\frac{1}{\eta}\quad \forall z\in CO,\forall z'\in CI \tag{18}$$

where $F_{z'}$ and $T_{z'}$ are the inlet flow rate and suction temperature, respectively; CO and CI are the output and input of the compressor, respectively; η is the isentropic efficiency; M_{gas} is the average molar weight; p_z and $p_{z'}$ are the pressures at suction and discharging flanges, respectively; and k is the compressor coefficient (set to be 1.4 in this paper) [28].

After preparing the feedstock gas (biogas and hydrogen) in terms of temperature and pressure, the reaction occurs in the methanation reactor to yield biomethane. The methane fraction within the biogas remains unchanged. Methanation involves two parallel reactions, i.e., reverse water-gas shift shown in (19) and Sabatier reactions shown in (20).

$$CO_{2(g)}+H_{2(g)}\leftrightarrow CO_{(g)}+H_2O_{(g)}\quad \Delta H=+41.5\ \text{kJ/mol} \tag{19}$$

$$CO_{(g)}+3H_{2(g)}\leftrightarrow CH_{4(g)}+H_2O_{(g)}\quad \Delta H=-206.2\ \text{kJ/mol} \tag{20}$$

Based on the stoichiometries of (19) and (20), the elementary balances for carbon, oxygen, and hydrogen atoms are respectively given by:

$$f_{CO_2,z'}=f_{CH_4,z}+f_{CO_2,z}+f_{CO,z}\quad \forall z\in RO,\forall z'\in RI \tag{21}$$

$$2f_{CO_2,z'}=2f_{CO_2,z}+f_{CO,z}+f_{H_2O,z}\quad \forall z\in RO,\forall z'\in RI \tag{22}$$

$$2f_{H_2,z'}=2f_{H_2,z}+4f_{CH_4,z}+2f_{H_2O,z}\quad \forall z\in RO,\forall z'\in RI \tag{23}$$

where RO and RI are the output and input of the reactor, respectively.

In addition, (19) and (20) should obey chemical equilibrium, where the relation between the temperature of the reactor T_r and partial pressure of each component p_c can be expressed by the equilibrium constant [29]:

$$\frac{1}{k_{wgs}}=10^{\frac{1910}{T_r}-1.784}=\frac{p_{CO}p_{H_2O}}{p_{CO_2}p_{H_2}} \tag{24}$$

$$\frac{1}{k_{met}}=10^{-\frac{11650}{T_r}+13.076}=\frac{p_{CH_4}p_{H_2O}}{p_{H_2}^3p_{CO}} \tag{25}$$

where subscripts wgs and met represent the reverse water-gas shift and Sabatier reactions, respectively.

Catalytical methanation is a highly exothermic reaction, and the heat released by the methanation reactor can be determined by the difference between the output and input streams as:

$$\dot{Q}_{reac}=\dot{Q}_z-\dot{Q}_{z'}\quad \forall z\in RO,\forall z'\in RI \tag{26}$$

The gas produced in the methanation reactor is saturated with water, which is removed. This procedure occurs in flash separation based on the liquid equilibrium. The separated water fraction is calculated as:

$$\ln\left(P_w\right) = A - \frac{B}{C+T} \tag{27}$$

$$K_{sep,w} = \varphi \frac{P_w}{P_{met}} \tag{28}$$

$$v_w = K_{sep,w} l_w \tag{29}$$

where A, B, and C are the Antoine parameters for water [30]; P_w and $K_{sep,w}$ are the vapor pressure (in mmHg) and gas-liquid equilibrium constant of water, respectively; φ is the conversion factor of pressure from atmospheres to millimeters of mercury; P_{met} is the pressure of methane; and v_w and l_w are the vapor and liquid states of water, respectively.

III. Problem Formulation and Solution

The MEC operates as an energy hub between upstream distributed energy grids and downstream energy consumers by incorporating different energy conversion units, enabling high-level flexible operation and cost reduction. We propose an optimal stochastic scheduling strategy for an MEC based on the models developed in Section II using mixed-integer nonlinear programming (MINP). The key values of the variables in the constraints are obtained from the MEC and PtM models during optimization. For example, the output gas flow of methanation g_t^{MET}, which is a key scheduling variable, can be obtained using (9) and (21)-(23), which represent the generated hydrogen flow and elementary balances of the reaction, respectively. In addition, the uncertainties of the RES output and energy loads are considered using a scenario-based algorithm.

A. Optimization Objective

The optimization objective is minimizing the TC of the MEC while considering all the technical constraints in every scenario. The TC for period Δt of the MEC includes the purchasing cost of electricity $p_{s,t}^G \lambda_t^{G,e}$, natural gas $g_{s,t}^G \lambda_t^{G,g}$, and biogas $b_{s,t}^G \lambda_t^{G,b}$ energy as well as the penalty cost caused by RES curtailment $c_R \Delta p_{s,res,t}^{cut}$, which is expressed as:

$$\min Z = \sum_{s=1}^{S} \pi_s \Delta t \left[\sum_{t=1}^{N} \left(p_{s,t}^G \lambda_t^{G,e} + g_{s,t}^G \lambda_t^{G,g} + b_{s,t}^G \lambda_t^{G,b} + c_R \Delta p_{s,res,t}^{cut} \right) \right] \tag{30}$$

where π_s is the probability of occurrence of each scenario; and N is the number of period Δt.

B. Constraints

The equality and inequality constraints in the MEC are given by (31)-(46). The subscripts of all the variables representing different scenarios are omitted for simplicity.

$$p_t^G + p_t^W + p_t^{PV} + g_t^{CHP} \eta_{ge} + p_t^{ES,out} = p_t^{EL} + p_t^{EHP} + p_t^{ES,in} + p_t^D \tag{31}$$

$$g_t^G + g_t^{MET} = g_t^D + g_t^{CHP} \tag{32}$$

$$g_t^{CHP} \eta_{gh} + h_t^{F,1} + h_t^{EHP} + h_t^{MET} = h_t^D \tag{33}$$

$$h_t^{F,2} \eta_{hc} + c_t^{EHP} = c_t^D \tag{34}$$

$$h_t^{F,1} + h_t^{F,2} = g_t^F \eta_F \tag{35}$$

$$h_t^{EHP} + c_t^{EHP} = p_t^{EHP} \cdot COP \tag{36}$$

$$\underline{g}^{CHP} \le g_t^{CHP} \le \bar{g}^{CHP} \tag{37}$$

$$c_t^{\min} I_t^c \le c_t^{EHP} \le c_t^{\max} I_t^c \tag{38}$$

$$h_t^{\min} I_t^h \le h_t^{EHP} \le h_t^{\max} I_t^h \tag{39}$$

$$I_t^h + I_t^c \le 1 \tag{40}$$

$$q_t^{ES} = q_{t-1}^{ES} + \left(p_t^{ES,in} \eta_{ES,in} - p_t^{ES,out} / \eta_{ES,out} \right) \Delta t \tag{41}$$

$$p_t^{ES,in} \le p_{\max}^{ES,in} I_t^{ES,in} \tag{42}$$

$$p_t^{ES,out} \le p_{\max}^{ES,out} I_t^{ES,out} \tag{43}$$

$$I_t^{ES,in} + I_t^{ES,out} \le 1 \tag{44}$$

$$SOC_{\min} \le SOC_t^{ES} \le SOC_{\max} \tag{45}$$

$$SOC_{t0} = SOC_{t24} \tag{46}$$

where the variables and coefficients in (31)-(46) are defined in Appendix A Tables AI and AII; η_{hc} and η_F are the efficiencies of the chiller boiler and gas furnace, respectively; $c_t^{\min}$ and $c_t^{\max}$ are the minimum and maximum cooling outputs of EHP, respectively; $h_t^{\min}$ and $h_t^{\max}$ are the minimum and maximum heat outputs of EHP, respectively; $p_{\max}^{ES,in}$ and $p_{\max}^{ES,out}$ are the maximum input and output power of ES, respectively; and $SOC_{\min}$ and $SOC_{\max}$ are the lower and upper limits of the SOC of ES, respectively. Equations (31)-(34) describe the power balance in terms of electricity, natural gas, heating, and cooling, respectively. The operation constraints of the furnace, EHP, and ES system are expressed by (35), (36)-(40), and (41)-(46), respectively.

C. Uncertainty Management

To describe the uncertainties introduced by the RESs (i.e., wind speed and solar irradiance) and loads (i.e., electricity, natural gas, heating, and cooling), a scenario-based stochastic method is adopted to reduce the computational complexity given the limited number of scenarios and known probability distributions of the uncertain parameters [31]. First, various scenarios containing the six parameters of the RESs and loads are generated using the Monte Carlo method based on the Rayleigh, Beta, and normal probability density functions [32]:

$$f\left(v_{s,t}\right) = \begin{cases} \dfrac{k}{\lambda} \left(\dfrac{v_{s,t}}{\lambda} \right)^{k-1} \mathrm{e}^{-\left(\frac{v_{s,t}}{\lambda}\right)^k} & v_{s,t} \ge 0 \\ 0 & v_{s,t} < 0 \end{cases} \tag{47}$$

$$f\left(r_{s,t}\right) = \begin{cases} \dfrac{\Gamma\left(\alpha+\beta\right)}{\Gamma\left(\alpha\right) + \Gamma\left(\beta\right)} r_{s,t}^{\alpha-1} \left(1-r\right)^{\beta-1} & 0 \le r_{s,t} \le 1 \\ 0 & \text{otherwise} \end{cases} \tag{48}$$

$$f_x\left(l_{x,s,t}\right) = \frac{1}{\sigma_x \sqrt{2\pi}} \exp\left(-\frac{\left(l_{x,s,t} - \mu_x\right)^2}{2\sigma_x^2} \right) \tag{49}$$

where $v_{s,t}$ is the speed of wind under every scenario; λ is a scale index equal to $2/\sqrt{\pi}\, v_{avg}$; v_{avg} is the average incident wind speed; k is the degree of freedom of $v_{s,t}$; r is the solar radiation quantified in kW/m^2; α and β are parameters of Beta distribution, defined by the average and standard deviation of solar radiation; $\Gamma(\cdot)$ is the Gamma function; x in (49) refers to electricity, natural gas, heat, and cold loads; $l_{x,s,t}$ is the consumer demand of x under every scenario; and μ_x and σ_x are the average and standard deviations of x, respectively.

After obtaining the stochastic wind speed and solar irradiance using (47) and (48) and the design parameters, the wind power and solar power are respectively calculated as [33]:

$$p^W(v)=\begin{cases} p^{Wr} & v_r \le v \le v_f \\ p^{Wr}\dfrac{v-v_c}{v_r-v_c} & v_c \le v < v_r \\ 0 & \text{otherwise} \end{cases} \tag{50}$$

$$p^{PV}(r)=\eta_{PV} S^{PV} r \tag{51}$$

where $p^W(v)$ is the output power of wind turbine; p^{Wr} is the rated power of wind turbine; v_f is the cut-out wind speed; v_r is the rated wind speed; v_c is the cut-in wind speed; $p^{PV}(r)$ is the output power of the photovoltaic system; η_{PV} is the efficiency of photovoltaic panels; and S^{PV} is the surface area of photovoltaic panels. Then, a vector of the six parameters, i.e., the maximum wind and solar output power as well as the power load, natural gas load, heating load, and cooling load in scenario s and stage t can be obtained with equal probability $1/N_S$ as:

$$\boldsymbol{X}_{s,t}=\left[p_{s,t}^{W,\max}\quad p_{s,t}^{PV,\max}\quad D_{s,t}^e\quad D_{s,t}^g\quad D_{s,t}^h\quad D_{s,t}^c\right] \tag{52}$$

where $p_{s,t}^{W,\max}$ is the maximum wind output power; $p_{s,t}^{PV,\max}$ is the maximum solar output power; $D_{s,t}^e$ is the power load; $D_{s,t}^g$ is the natural gas load; $D_{s,t}^h$ is the heating load; and $D_{s,t}^c$ is the cooling load. Subsequently, the SCENRED2 scenario reduction algorithm, which is based on the fast backward method [34], is employed to optimally reduce the number of scenarios. Thus, the accuracy of the scheduling results and computational burden can be balanced.

Overall, the proposed optimal stochastic scheduling of the MEC is achieved by solving (4)-(18) with constraints given by (21)-(46) and the objective function given by (30):

$$\begin{cases} \min Z \\ \text{s.t. PtM constraints (4)-(18), (21)-(29)} \\ \qquad \text{MEC constraints (31)-(46)} \end{cases} \tag{53}$$

The proposed model is formulated using MINP and can be solved using a variety of solvers and commercial software such as GAMS [35], AIMMS [36], and LINGO [37]. In this paper, we used the BONMIN and KNITRO solvers from GAMS.

IV. Case Studies

We evaluated case studies considering a rural MEC to demonstrate the effectiveness of the proposed optimal stochastic scheduling strategy.

A. Test System and Parameters

The design assumptions for the energy conversion facilities and other parameters within the MEC are presented in Appendix A. The considered time-varying electricity prices are shown in Fig. 4. The forecasts of loads, wind speed, and solar irradiance on a typical winter day are shown in Fig. 5 and follow the data in [32] and [38] with minor modifications. Based on the forecasting data and corresponding probability distribution functions, 100 scenarios were randomly generated. SCENRED2 was used to obtain three representative scenarios with the probabilities listed in Table I. We also considered 10 scenarios in Section IV-D.

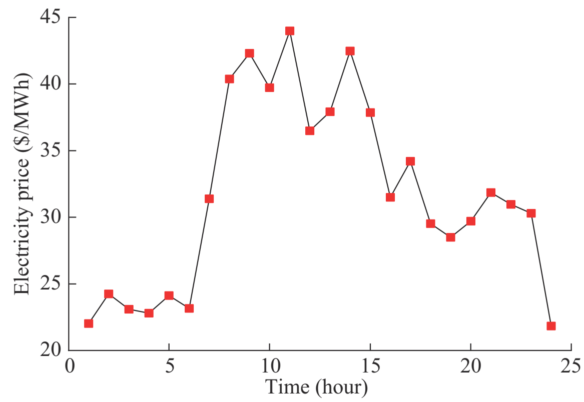

Fig. 4. Time-varying electricity prices considered in this paper.

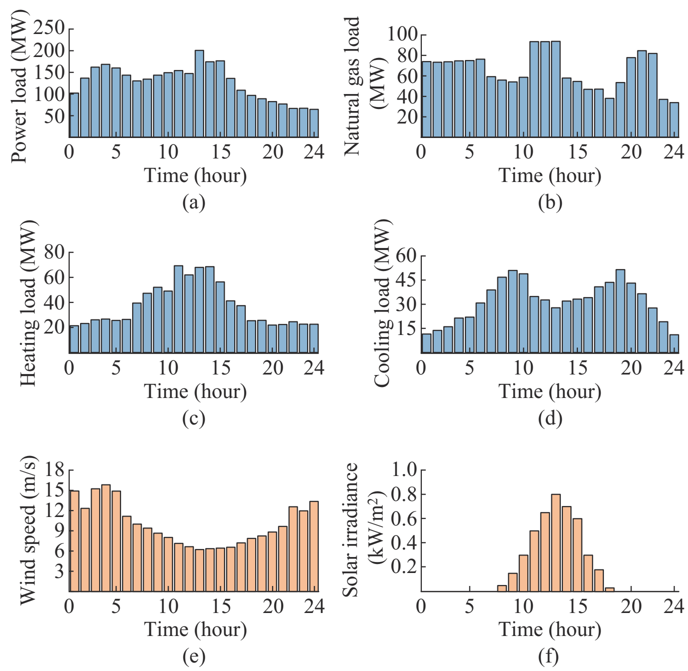

Fig. 5. Forecasts of loads, wind speed, and solar irradiance, on a typical winter day. (a) Power load. (b) Natural gas load. (c) Heating load. (d) Cooling load. (e) Wind speed. (f) Solar irradiance.

TABLE I
PROBABILITIES OF THREE REPRESENTATIVE SCENARIOS

Scenario No.	Probability
1	0.19
2	0.28
3	0.53

B. Effectiveness of Proposed Strategy

For clarity and simplicity, we report the scheduling results for scenario 3. Figures 6-8 show that with the coordinated scheduling of energy conversion units (i.e., PtM unit, CHP unit, EHP, gas furnace, chiller boiler, and ES), the supply and demand of electrical, natural gas, heating, and cooling energy are balanced. Positive values represent purchased, generated, or discharged energy, and negative values represent consumed or charged energy. W_{cur} is the power of wind curtailment and F is the power of furance.

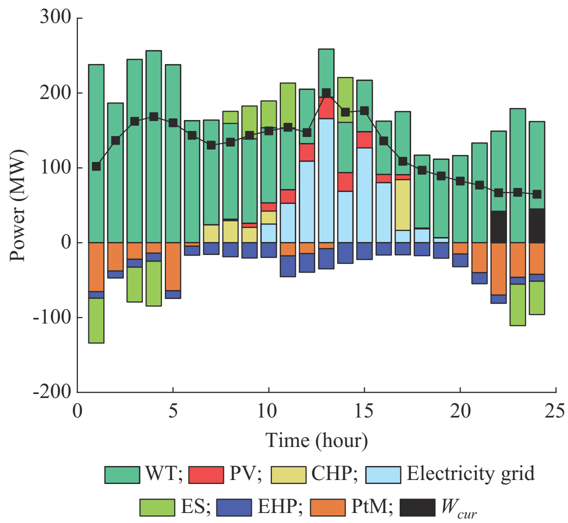

Fig. 6. Scheduling strategies for electrical power.

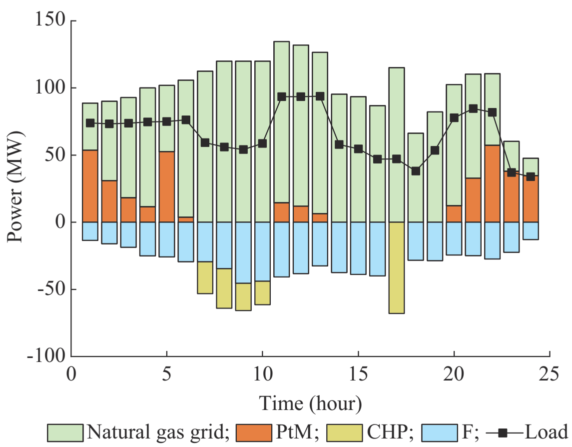

Fig. 7. Scheduling strategies for natural gas.

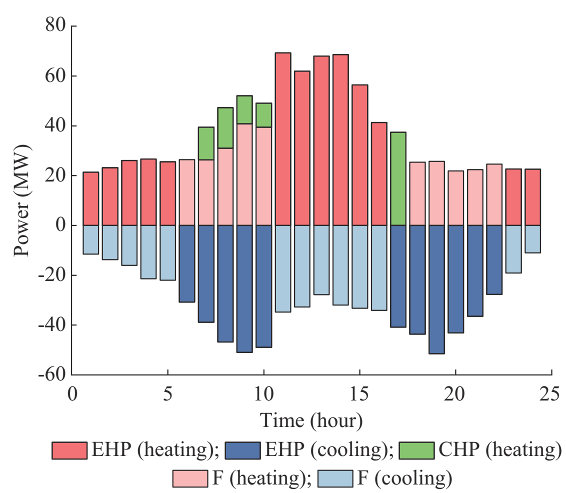

Fig. 8. Scheduling strategies for heating and cooling.

From Figs. 6-8, the following findings are obtained.

1) Electric power is supplied by RES generation (wind and solar energy), the CHP unit, ES system, and upper power grid.

From hour 10 to hour 19 in Fig. 6, the MEC must purchase electricity (approximately 670 MW) from the electricity grid because of insufficient wind power. However, as the heat and gas demands are higher in winter than in other seasons, a larger power consumption of the EHPs and lower power supply from the CHP unit occur. Wind curtailment only occurs at hour 22 and hour 24 (42.15 MW and 45.3 MW, respectively) because electricity is at off-peak periods and the PtM unit already operates at full load.

2) As illustrated in Fig. 6, the utilization rate of the electrolyzer is approximately 60%. Specifically, it is activated from hour 1 to hour 16 and from hour 20 to hour 24 to consume the surplus wind generation, while 40.14 MW methane should be provided by the PtM unit because the natural gas supply from the distribution network reaches its upper limit.

3) As shown in Fig. 7, natural gas is primarily provided by the upstream distribution network and supplied to the furnace and gas demand. Owing to the relatively low heat production efficiency of the CHP unit compared with the furnace and high cost of power production compared with the EHP, gas energy is only used to operate the CHP unit during hour 7 to hour 10 and hour 17.

4) As shown in Fig. 8, the cooling demand is provided by the EHP and furnace, while the heating demand is satisfied by the CHP unit, except for these two facilities. Because the EHP can only operate for heating or cooling at a time, both loads should be covered by an alternate EHP and furnace. In addition, approximately 9.7% of the heating demand is supported by the CHP unit under insufficient electricity and heating supply.

Figures 9 and 10 show the optimized strategies and performance of methane synthesis. Figure 9 shows the biomethane and heat production for methane synthesis, including the heat released by the methanation reactor and heat exchangers, which increases with the biomethane production. In addition, the highest biomethane production rate occurs at around hour 20 (57.33 MW) owing to the excess wind generation and high natural gas load.

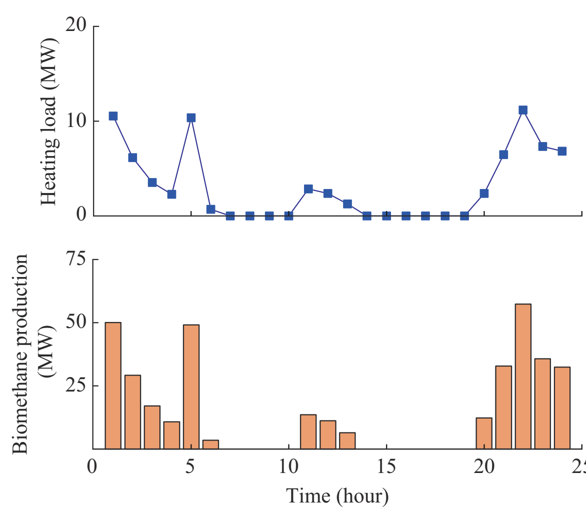

Fig. 9. Biomethane and heat production for methane synthesis.

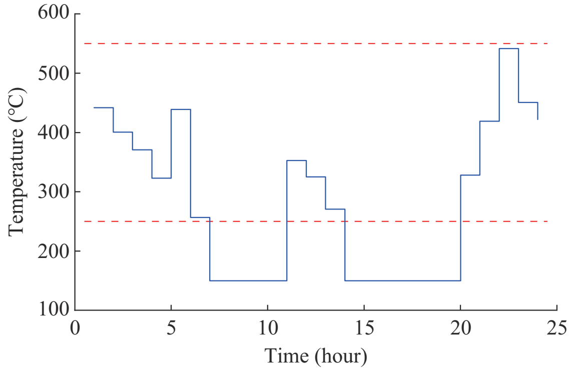

Fig. 10. Temperature variation of PtM process.

The temperature variation of PtM process is shown in Fig. 10. The reactor temperature consistently follows the variation in power consumption of the PtM unit. Around hour 20, the peak hydrogen energy input should account for the highest operating temperature of methanation reactor (around 541.33 ℃). The average temperature of the methanation reactor is around 377 ℃. Optimizing the temperature allows to improve the conversion rate of methane.

The average selectivity, which reflects the mass fraction of biomethane in the product gas, can be defined as:

$$\bar{\beta}=\frac{\left(n_b-n_{b0}\right)/b}{\left(n_{h0}-n_h\right)/h} \tag{54}$$

where n_{b0}, n_{h0}, n_b, and n_h are molar weights of biomethane and hydrogen at the beginning and end of the reaction, respectively; and b and h are the stoichiometric coefficients of methane and hydrogen, respectively.

Figure 11 shows the average selectivity of the methanation synthesis. A proper flowsheet design and optimized temperature for the methanation reactor allow the average selectivity of methane throughout the day to reach 83.7%, with all values being higher than 80% and the highest value reaching 90.2% at hour 6, when the power consumption of the PtM unit (4.45 MW) is the lowest.

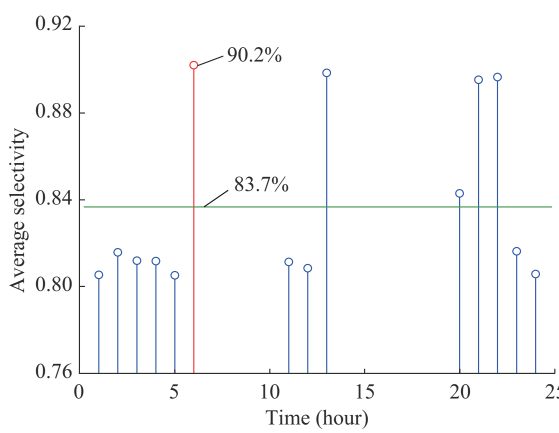

Fig. 11. Average selectivity of methane synthesis.

C. Sensitivity Analysis

Recently, the price of natural gas has increased mainly owing to political factors. Therefore, we investigated the response of the proposed MEC operation strategy to the changes in natural gas price. Figure 12 shows that the variation in electricity and natural gas procurement changes slowly when the gas price is lower than 30 \$/MWh and then increases and decreases rapidly to remain unchanged when it rises to 60 \$/MWh. This is because a certain amount of energy must be supplied from the upper distribution network to fulfill various types of loads.

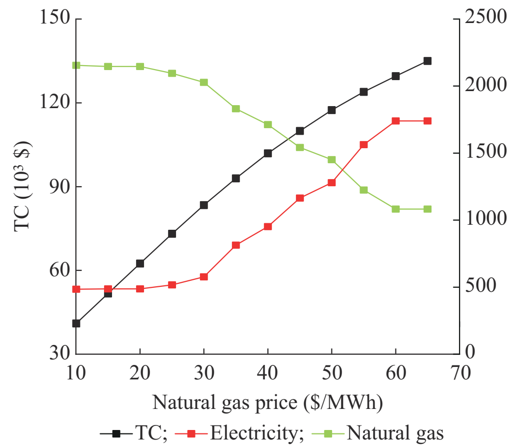

Fig. 12. Impacts of natural gas price on TC and energy consumption of electricity and natural gas.

As gas supply capacity in a rural area is constrained by incomplete facilities and geographical factors, the impacts of the gas supply capacity on the TC and energy consumption of the PtM and CHP units were also explored. The results are shown in Fig. 13. The gas supply capacity of 130 MW is the inflection point, after which the total cost changes slowly. In addition, the energy consumption of the PtM and CHP units first varies rapidly with the gas supply capacity, and then increases slightly when it exceeds 130 MW and 150 MW, respectively.

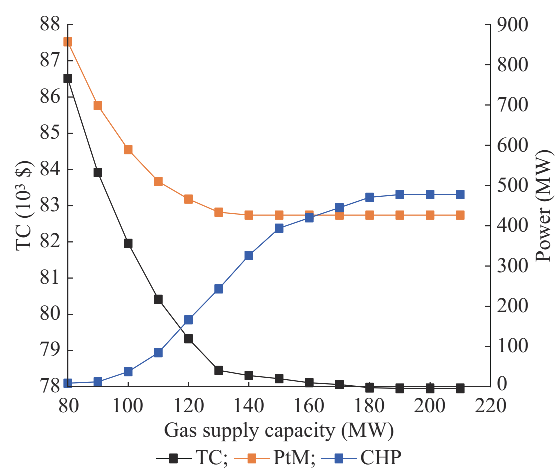

Fig. 13. Impact of gas supply capacity on TC and energy consumption of PtM and CHP units.

D. Verification for Multiple Scenarios

Owing to the complexity of scheduling, 100 scenarios generated by the Monte Carlo method were reduced to three representative scenarios to simplify computations, which might be insufficient to demonstrate the viability of the proposed strategy. Thus, we also reduced the original 100 scenarios to 10 scenarios and evaluated the average selectivity of methane synthesis to validate the results with the three representative scenarios. Based on the generated 100 scenarios, SCENRED2 was used to reduce the number of scenarios to 10. The probabilities of the 10 scenarios are listed in Table II. The weighted average selectivity for methane synthesis are shown in Fig. 14. After expanding the scenarios, the average methane selectivity throughout the day is 84.2%, with all values being higher than 80%, and the highest value being 90.8%. There are no discrepancies compared with Fig. 11 (e.g., the difference in the average is only 0.5%). Thus, the results with three scenarios in Section IV-A are representative, and the feasibility of the proposed strategy was verified.

TABLE II
PROBABILITIES OF 10 SCENARIOS FOR EXTENDED EVALUATION

Scenario No.	Probability	Scenario No.	Probability
1	0.164	6	0.101
2	0.149	7	0.082
3	0.128	8	0.068
4	0.126	9	0.064
5	0.102	10	0.016

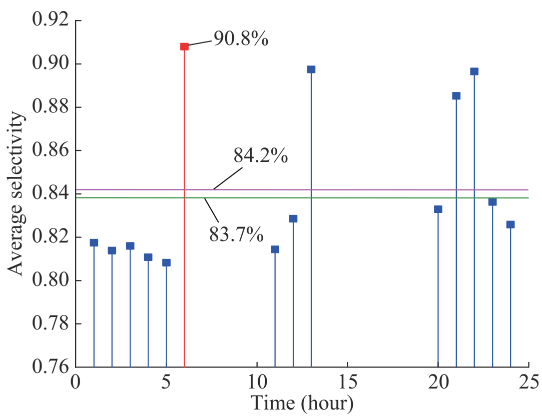

Fig. 14. Average selectivity of methane synthesis for 10 scenarios.

V. CONCLUSION

We propose an optimal stochastic scheduling strategy for an MEC integrated with a full-blown PtM model considering reactor kinetics and chemical equilibria. To minimize the TC, the scheduling captures the temperature variations in the methanation reactor and maximizes the average selectivity for biomethane. Numerical analyses have been performed considering a rural MEC. Our key findings and contributions are summarized as follows.

1) A concise PtM model is derived and integrated into an MEC, bridging the gap between the complexity of chemical processes and systematic analysis of methanation. This integration enables the PtM process to be scheduled from an overall system perspective and may improve the controllability of the PtM unit for MEC operators, thus enhancing the MEC operation flexibility.

2) A stochastic scheduling strategy for an MEC is introduced considering the PtM model and uncertainties to minimize the TC. The optimal scheduling strategy for electricity, natural gas, heating, and cooling is obtained. The strategy may promote the optimal operation of power grid companies to regulate PtM plants, including electrolyzers and methanation reactors, in the future.

3) The optimized performance of methane synthesis, power consumption of the PtM unit, and temperature of the methanation reactor is achieved. In addition, a sensitivity analysis reveals the change in MEC operation strategy according to the natural gas price and the impact of the gas supply capacity on the TC. The sensitivity analysis may provide guidance to MEC operators about strategies to be adopted in advance and to natural gas companies about investments in natural gas facilities, as the TC and energy consumption of the PtM and CHP units are considerably sensitive to the gas supply capacity.

In future work, we will focus on the operation strategy of MEC considering the cascading heat utilization between a solid oxide electrolyzer cell and methanation reactor as well as the corresponding flowsheet design and modeling.

APPENDIX A

TABLE AI
DEFINITION OF VARIABLES FOR SCHEDULING

Variable	Description	Unit
p_t^G	Electricity power from the grid	MW
p_t^W	Wind power	MW
p_t^{PV}	Solar power	MW
$p_t^{ES,out}$	Output power of ES in discharging state	MW
p_t^{EL}	Power consumption of electrolyzer	MW
p_t^{EHP}	Power consumption of EHP	MW
$p_t^{ES,in}$	Input power of ES in charging state	MW
g_t^G	Output natural gas flow from the gas grid	kg/s
g_t^{MET}	Output natural gas flow from PtM model	kg/s
g_t^{CHP}	Natural gas consumption of CHP	kg/s
g_t^F	Natural gas consumption of furnace	kg/s
h_t^{EHP}	Heating output of CHP	MW
h_t^{MET}	Heating output of MET	MW
$h_t^{F,1}$	Heating output to demand of furnace	MW
$h_t^{F,2}$	Heating output to CB of furnace	MW
c_t^{EHP}	Cooling output of EHP	MW
q_t^{ES}	Quantity of electric charge of the ES	C
SOC_t^{ES}	SOC of ES at the time t	%
$SOC_{t_0}^{ES}$, $SOC_{t_{24}}^{ES}$	SOC of ES at the time t_0 and t_{24}	%
I_t^c	Signal for operating mode of EHP (EHP operates at refrigerating mode if $I_t^c=1$, or the refrigerating system of EHP is out of service if $I_t^c=0$)	
I_t^h	Signal for operating mode of EHP (EHP operates at heating mode if $I_t^h=1$, or the heating system of EHP is out of service if $I_t^h=0$)	
$I_t^{ES,in}$	Signal for operating mode of ES (ES operates at charging mode if $I_t^{ES,in}=1$, or the charging system of ES is out of service if $I_t^{ES,in}=0$)	
$I_t^{ES,out}$	Signal for operating mode of ES (ES operates at discharging mode if $I_t^{ES,out}=1$, or the discharging system of ES is out of service if $I_t^{ES,out}=0$)	

TABLE AII
DEFINITIONS AND VALUES OF INPUT DATA FOR SCHEDULING

Parameter	Description	Unit	Value
$\lambda_t^{G,e}$	Electricity price	\$/MWh	Time-varying as shown in Fig. 4
$\lambda_t^{G,g}$	Natural gas price	\$/kg	0.78
$\lambda_t^{G,b}$	Biogas price	\$/kg	0.12
c_R	Penalty cost for RES curtailment	\$/MWh	71.43
p_t^D	Power consumption demand	MW	Time-varying as shown in Fig. 5
g_t^D	Natural gas consumption demand	MW	Time-varying as shown in Fig. 5
h_t^D	Heating consumption demand	MW	Time-varying as shown in Fig. 5
c_t^D	Cooling consumption demand	MW	Time-varying as shown in Fig. 5
s^{PV}	Area of PV panels	m^2	64
p^{Wcap}	Capacity of wind turbines	MW	100
$\bar{p}^{EL}$	Electrolyzer	MW	40
$\bar{g}^{CB}$	Chiller boiler	MW	55
$\bar{g}^{F}$	Furnace	MW	55
$\bar{g}^{CHP}$, $\underline{g}^{CHP}$	The maximum and minimum power consumptions of CHP	MW	55, 0
$\bar{p}^{EHP}$	Electric heat pump	MW	30
$\bar{q}^{ES}$	Electricity storage system	MW	300
COP	Coefficient of performance of electric heat pump	MW	2.5
η_{ge}	CHP efficiency for natural gas to electricity		0.35
η_{gh}	CHP efficiency for natural gas to heat		0.55
η_F	Furnace efficiency		0.9
η_{hc}	Chiller boiler efficiency		0.95
$\eta_{ES,in}$, $\eta_{ES,out}$	Battery charging and discharging efficiencies		0.9, 0.9

REFERENCES

[1] H. Hui, M. Bao, Y. Ding *et al*., "Optimal energy reserve scheduling in integrated electricity and gas systems considering reliability requirements," *Journal of Modern Power Systems and Clean Energy*, vol. 10, no. 6, pp. 1494-1506, Nov. 2022.

[2] BP. (2021, Jul.) Statistical review of world energy. [Online]. Available: https://www.bp.com/

[3] Q. Li, R. Li, Y. Pu *et al*., "Coordinated control of electric-hydrogen hybrid energy storage for multi-microgrid with fuel cell/electrolyzer/PV/battery," *Journal of Energy Storage*, vol. 42, p. 103110, Oct. 2021.

[4] Z. Zhang, C. Wang, H. Lv *et al.*, "Day-ahead optimal dispatch for integrated energy system considering power-to-gas and dynamic pipeline networks," *IEEE Transactions on Industry Applications*, vol. 57, no. 4, pp. 3317-3328, Jul.-Aug. 2021.

[5] J. Salehi, A. Namvar, F. S. Gazijahani *et al.*, "Effect of power-to-gas technology in energy hub optimal operation and gas network congestion reduction," *Energy*, vol. 240, p. 122835, Feb. 2022.

[6] S. M. Alirahmi, E. Assareh, A. Chitsaz *et al.*, "Electrolyzer-fuel cell combination for grid peak load management in a geothermal power plant: Power to hydrogen and hydrogen to power conversion," *International Journal of Hydrogen Energy*, vol. 46, no. 50, pp. 25650-25665, Jul. 2021.

[7] S. Amiri, M. Honarvar, and A. sadegheih, "Providing an integrated model for planning and scheduling energy hubs and preventive maintenance," *Energy*, vol. 163, pp. 1093-1114, Nov. 2018.

[8] X. Dong, J. Wu, Z. Xu *et al.*, "Optimal coordination of hydrogen-based integrated energy systems with combination of hydrogen and water storage," *Applied Energy*, vol. 308, p. 118274, Feb. 2022.

[9] F. Gutiérrez-Martín, L. M. Rodríguez-Antón, and M. Legrand, "Renewable power-to-gas by direct catalytic methanation of biogas," *Renewable Energy*, vol. 162, pp. 948-959, Dec. 2020.

[10] F. M. Baena-Moreno, Z. Zhang, X. Zhang *et al.*, "Profitability analysis of a novel configuration to synergize biogas upgrading and power-to-gas," *Energy Conversion and Management*, vol. 224, p. 113369, Nov. 2020.

[11] Y. Yin, T. Liu, L. Wu *et al.*, "Day-ahead risk-constrained stochastic scheduling of multi-energy system," *Journal of Modern Power Systems and Clean Energy*, vol. 9, no. 4, pp. 720-733, Jul. 2021.

[12] X. Cao, X. Sun, Z. Xu *et al.*, "Hydrogen-based networked microgrids planning through two-stage stochastic programming with mixed-integer conic recourse," *IEEE Transactions on Automation Science and Engineering*, vol. 19, no. 4, pp. 3672-3685, Oct. 2022.

[13] Z. Wang, J. Hu, and B. Liu, "Stochastic optimal dispatching strategy of electricity-hydrogen-gas-heat integrated energy system based on improved spectral clustering method," *International Journal of Electrical Power & Energy Systems*, vol. 126, p. 106495, Mar. 2021.

[14] A. Fache, F. Marias, V. Guerré *et al.*, "Optimization of fixed-bed methanation reactors: safe and efficient operation under transient and steady-state conditions," *Chemical Engineering Science*, vol. 192, pp. 1124-1137, Dec. 2018.

[15] E. Giglio, R. Pirone, and S Bensaid, "Dynamic modelling of methanation reactors during start-up and regulation in intermittent power-to-gas applications," *Renewable Energy*, vol. 170, pp. 1040-1051, Jun. 2021.

[16] R Bedoić, H Dorotić, D. R Schneider *et al.*, "Synergy between feedstock gate fee and power-to-gas: an energy and economic analysis of renewable methane production in a biogas plant," *Renewable Energy*, vol. 173, pp. 12-23, Aug. 2021.

[17] K. L. Fischer and H. Freund, "On the optimal design of load flexible fixed bed reactors: Integration of dynamics into the design problem," *Chemical Engineering Journal*, vol. 393, p. 124722, Aug. 2020.

[18] C. Dannesboe, J. B. Hansen, and L. Johannsen, "Catalytic methanation of CO2 in biogas: experimental results from a reactor at full scale," *Chemical Engineering Journal*, vol. 5, pp. 183-189, Nov. 2019.

[19] J. Han and C. Liu, "Performance evaluation of SSCI damping controller based on the elastic energy equivalent system," *Applied Energy*, vol. 331, p. 120270, Feb. 2023.

[20] C. Liu and J. Han, "Evaluation of the sub-synchronous control interaction based on the elastic energy equivalent system," *IEEE Transactions on Power Systems*, vol. 38, no. 4, pp. 3897-3910, Jul. 2023.

[21] L. Shang, Z. Hua, C. Liu *et al.*, "Amplitude-phase-locked-loop-based power injection strategy for wind power generation under three-phase grid fault," *IEEE Transactions on Energy Conversion*, vol. 37, no. 4, pp. 2952-2961, Dec. 2022.

[22] L. Shang, X. Dong, C. Liu *et al.*, "Fast grid frequency and voltage control of battery energy storage system based on the amplitude-phase-locked-loop," *IEEE Transactions on Smart Grid*, vol. 13, no. 2, pp. 941-953, Mar. 2022.

[23] M. S. Ghafoori, K. Loubar, M. M. Gallego *et al.*, "Techno-economic and sensitivity analysis of biomethane production via landfill biogas upgrading and power-to-gas technology," *Energy*, vol. 239, p. 122086, Jan. 2022.

[24] J. D. Fonseca, J. M. Commenge, M. Camargo *et al.*, "Multi-criteria optimization for the design and operation of distributed energy systems considering sustainability dimensions," *Energy*, vol. 214, p. 118989, Jan. 2021.

[25] K. Hjuler and N. Aryal, "Review on biogas upgrading – future gas project, WP1," Danish Gas Technology Centre, Hørsholm, Denmark, Rep. 742-55, Sept. 2017.

[26] J. Li, G. Li, S. Ma *et al*., "Modeling and simulation of hydrogen energy storage system for power-to-gas and gas-to-power systems," *Journal of Modern Power Systems and Clean Energy*, vol. 11, no. 3, pp. 885-895, May 2023.

[27] R. Keller, E. Rauls, M. Hehemann *et al.*, "An adaptive model-based feedforward temperature control of a 100 kW PEM electrolyzer," *Control Engineering Practice*, vol. 120, p. 104992, Mar. 2022.

[28] S. Mokhatab, A. W. Poe, and G. J. Speight, *Handbook of Natural Gas Transmission and Processing*, 4th ed., Houston: Joe Hayton, 2019.

[29] D. Uysal, "Equilibrium analyses and kinetics of carbon dioxide methanation using an alumina-supported ruthenium catalyst," *Chemical Engineering Technology*, vol. 44, no. 10, pp. 1939-1946, Sept. 2021.

[30] R. K. Sinnott, "Coulson & Richardson's chemical engineering," in *Chemical Engineering*, 3rd ed., vol. 6, Burlington: Butterworth-Heinemann, 1999, pp. 947-967.

[31] L. Hao, J. Ji, D. Xie *et al.*, "Scenario-based unit commitment optimization for power system with large-scale wind power participating in primary frequency regulation," *Journal of Modern Power Systems and Clean Energy*, vol. 8, no. 6, pp. 1259-1267, Nov. 2020.

[32] M. H. Shams, M. Shahabi, M. Kia *et al.*, "Optimal operation of electrical and thermal resources in microgrids with energy hubs considering uncertainties," *Energy*, vol. 187, p. 115949, Nov. 2019.

[33] Y. Liu, D. Liu, and H. Zhang, "Stochastic unit commitment with high-penetration offshore wind power generation in typhoon scenarios," *Journal of Modern Power Systems and Clean Energy*, vol. 12, no. 2, pp. 535-546, Mar. 2024.

[34] H. Heitsch and W. Römisch, "A note on scenario reduction for two-stage stochastic programs," *Operations Research Letters*, vol. 35, no. 6, pp. 731-738, Nov. 2007.

[35] GAMS Development Corporation. (1988, Dec). GAMS, a user's guide. [Online]. Available: https://www. gams. com/latest/docs/UG_MAIN.pdf

[36] AIMMS. (2022, Oct.). Optimization modeling. [Online]. Available: https://documentation.aimms.com/_downloads/AIMMS_modeling.html

[37] LINGOS. (2020, Dec.). User's manual. [Online]. Available: https://www.lindo.com/downloads/PDF/LINGO.pdf

[38] J. Hu, X. Liu, and C. Wang, "Value evaluation of energy hub flexibility considering network constraints," *Proceedings of the CSEE*, vol. 42, no. 5, pp. 1799-1812, Mar. 2022.

Guanwei Zeng received the B.E. degree in electrical engineering from Wuhan University, Wuhan, China, in 2021. He is currently working toward the M.S. degree in electrical engineering at the School of Electrical Engineering and Automation, Wuhan University. His research interests include renewable energy integration, network stability, and multi-energy systems.

Chengxi Liu received the B.S. and M.S. degrees in electrical engineering from Huazhong University of Science and Technology, Wuhan, China, in 2005 and 2007, respectively, and the Ph.D. degree from Aalborg University, Aalborg, Denmark, in 2013. He was a Power System Analyst with Energinet.dk (the Danish TSO) until 2016, and a Research Associate with the University of Tennessee, Knoxville, USA, from 2016 to 2018. He was an Associate Professor with the Department of Energy Technology, Aalborg University. He is currently a Full Professor with the School of Electrical Engineering and Automation, Wuhan University, Wuhan, China. His research interests include power system stability and analysis, simulation methods for power systems, and multi-energy systems.

Minfang Liao received the B.E. degree in electrical engineering and its automation from Shenyang Jianzhu University, Shenyang, China, in 2013, and the M.Sc. degree in electrical engineering from Sichuan University, Chengdu, China, in 2017. She is currently pursuing the Ph.D. degree in electrical engineering in Wuhan University, Wuhan, China. Her research interest includes optimal operation of multi-energy systems.

Yongjian Luo received the B.E. degree in electrical engineering from Shandong University, Jinan, China, in 2018. He is currently pursuing the Ph.D. degree in School of Electrical Engineering and Automation, Wuhan University, Wuhan, China. His research interests include power system analysis, power flow calculation, and voltage stability analysis.

Xuzhu Dong received the M.S. and Ph.D. degrees from Tsinghua University, Beijing, China, in 1995 and 1998, respectively, and the second Ph.D. degree from Virginia Tech, Blacksburg, USA, in 2002. He is a Professor and the Dean of the School of Electrical Engineering and Automation, Wuhan University, Wuhan, China. He was the Deputy Chief Engineer and the Director of the Smart Grid Institute of China Southern Power Grid (CSG) Electric Power Research Institute (EPRI), Guangzhou, China. Before joining CSG, he worked with Progress Energy, FirstEnergy, and EPRI solutions in USA, as a Senior Engineer, Stuff Engineer, and Lead Engineer, respectively. He is a Member of CIGRE. His research interests include smart distributions, microgrids, integration of renewable energy, energy storage, and asset management.